Thermal Decomposition and Isomerization Processes of Alkyl Radicals

Noboru Yamauchi, Akira Miyoshi,* Keishi Kosaka, Mitsuo Koshi, and Hiroyuki Matsui

Department of Chemical System Engineering, The University of Tokyo, 7-3-1, Hongo, Bunkyo-ku, Tokyo 113-8656, Japan

Received: November 17, 1998; In Final Form: February 2, 1999

The thermal decomposition and isomerization processes of C_3-C_4 alkyl radicals, 1-C_5H_{11}, and 1-C_6H_{13} have been investigated by using a shock-tube apparatus coupled with atomic resonance absorption spectrometry (ARAS). Isomeric alkyl radicals were generated by the thermal decomposition of respective alkyl iodides. Branching fractions for the competitive pathways (C−C bond cleavage, C−H bond cleavage, and isomerization) have been determined by following the hydrogen-atom concentration by ARAS. In the investigated temperature range (900−1400 K), for all alkyl radicals, the energetically favored C−C bond cleavage was found to dominate over the C−H bond cleavage. The 1,2 or 1,3 isomerization reaction was found to be minor in C_3 and C_4 alkyl radicals. On the other hand, the results for 1-C_5H_{11} and 1-C_6H_{13} radicals clearly show the occurrence of 1,4 and 1,5 isomerization reactions. From an RRKM analysis of the present result and the previous lower temperature data, with consideration of the tunneling effect, the threshold energies for 1,4 and 1,5 primary-to-secondary isomerization reactions were evaluated to be 21.5 ± 1.2 and 14.6 ± 1.2 kcal mol^{-1}, respectively. The high-pressure limit rate constants for the isomerization processes were evaluated as k^{∞}(1-C_5H_{11} → 2-C_5H_{11}) = $4.88 \times 10^8 T^{0.846}$ exp(−19.53 [kcal mol^{-1}]/RT) s^{-1} and k^{∞}(1-C_6H_{13} → 2-C_6H_{13}) = $6.65 \times 10^7 T^{0.823}$ exp(−12.45 [kcal mol^{-1}]/RT) s^{-1} for the temperature range 350−1300 K. Even under relatively high-pressure conditions (∼1 atm), the falloff effect was shown to be important for multichannel dissociation systems. The nonequilibrium effect in the thermal decomposition of energized alkyl radicals formed in the high-temperature reaction system, which has been first suggested by Tsang et al. [*J. Phys. Chem.* **1996**, *100*, 4011] was discussed. The possible effect of the tunneling in the isomerization reactions was discussed in comparison with previous lower temperature data.

Introduction

Thermal decomposition of alkyl radicals plays an important role in the combustion of hydrocarbons. It is one of the important elementary reactions in the oxidation processes of alkanes, and it competes with the reaction with O_2, especially at high temperatures and under fuel-rich conditions. Recently, Gutman, Slagle, and co-workers have investigated the thermal decomposition of C_2 to C_4 alkyl radicals at low temperatures (<1100 K) and at low pressures (<20 Torr) with a laser photolysis−photoionization mass spectrometry method.[1] Under their experimental conditions, the dominant product channel was confirmed to be, or assumed to be, the energetically most favored channel (in many cases, the C−C bond fission channel). However, at elevated temperatures, energetically less favored reaction channel (for example, C−H bond fission channel) may open up. Rate parameters for these minor channels have been derived[2−5] from the analysis of chain reaction system or estimated from the rate parameters for reverse reactions measured at lower temperatures, but experimental information at high temperatures is limited.

Furthermore, for long-chain alkyl radicals, the isomerization processes are known to compete with the direct dissociation processes.[6] Earlier experiments[7] have been reviewed by Benson,[8] who explained the occurrence of five-membered ring isomerization[7a,b] and the lack of evidence for three- or four-membered ring isomerizations[7b] with the estimated activation energies and preexponential factors (*A* factors) based on the ring strain energies and the hindrance of internal rotations in the transition states. Abnormally low *A* factors (10^7-10^8 s^{-1}) for five- or six-membered ring isomerization reported earlier[7c,9] have been shown to be too low.[10] Several experimental investigations have been also reported for three- or four-membered ring isomerization.[11] Although some earlier investigations on the three- or four-membered ring isomerization indicated low activation energies or large fractions for these processes, recent investigations showed higher threshold energies[11g,h] close to, or higher than, that for C−H fission (∼34 kcal mol^{-1}). Several quantum chemical calculations on the three-membered ring transition state of ethyl radical,[12] and on three- to seven-membered ring transition states of larger alkyl radicals[13] also support the high ring strain energies for three- or four-membered ring transition states. Isomerization via five- and six-membered ring transition states was also reported for the energized alkyl radicals produced by the photolysis of haloalkanes in the collision-free molecular-beam conditions.[14] Since most of the rate parameters for isomerization processes have been derived from the analysis of chain reaction systems and sometimes suffered from the reaction mechanism assumed,[10a] direct observations of the isomerization processes are needed.

In the present study, the branching fractions for the thermal decomposition of *n*-C_3H_7, *i*-C_3H_7, *n*-C_4H_9, *s*-C_4H_9, *i*-C_4H_9, 1-C_5H_{11}, and 1-C_6H_{13} were investigated at elevated temperatures (900−1400 K) by a shock tube apparatus with direct and quantitative measurements of product hydrogen atoms, in order to investigate the possible contribution of higher C−H bond fission channels, and to investigate the isomerization processes in competition with C−C bond fission reactions.

10.1021/jp9844563 CCC: $18.00 © 1999 American Chemical Society
Published on Web 03/19/1999

Experimental Section

Details of the shock tube apparatus have been described previously.[13] Briefly, a diaphragmless stainless steel shock tube (5 cm i.d. and 4 m long) with an ARAS (atomic resonance absorption spectrometry) detection system was used in the present study. A microwave discharge in a flowing gas mixture of 1% H_2/He or 0.1% I_2/He was used as a light source for the ARAS measurement of H or I atoms, respectively. Atomic transitions from the lamp, 121.6 nm [^2P-$^2S_{1/2}$(2p−1s)] for H or 183.0 nm [$^4P_{5/2}$-$^2P_{3/2}$(6s−5p)] for I, were filtered with a 20 cm vacuum-UV monochromator and detected by a solar-blind photomultiplier. The ARAS calibration for H and I atoms was performed using the thermal decomposition of methyl iodide and ethyl iodide, respectively.

Isomeric alkyl radicals were generated by the thermal decomposition of respective alkyl iodides,

$$RI + M \rightarrow R + I + M \quad (1a)$$

$$\rightarrow \text{alkene} + HI + M \quad (1b)$$

Since molecular dissociation channel 1b is possible in the thermal decomposition of alkyl iodides, the initial concentration of alkyl radicals was determined by following the concentration of iodine atoms, counterpart of the alkyl radicals, by ARAS. Branching fractions for the competitive dissociation or isomerization pathways were determined by following the hydrogen atom concentrations by ARAS. For the quantitative measurement of hydrogen atoms, experiments were performed alternately with the thermal decomposition of ethyl iodide,

$$C_2H_5I + M \rightarrow C_2H_5 + I + M \quad (2a)$$

$$\rightarrow C_2H_4 + HI + M \quad (2b)$$

for which the branching fraction has been measured precisely by Kumaran et al.[14] (87% for reaction 2a). The thermal decomposition of the ethyl radical

$$C_2H_5 + M \rightarrow C_2H_4 + H + M \quad (3)$$

after reaction 2a, was used as a reference reaction for the hydrogen atom concentration.

The gases used were obtained from Nihon Sanso (He, >99.9999%; Ar, >99.9999%; H_2, >99.9999%), Wako (I_2, 99.9%; CH_3I, >99%; n-C_3H_7I, >97%; i-C_3H_7I, >99%), and Tokyo Kasei (C_2H_5I, >99%; n-C_4H_9I, >98%; s-C_4H_9I, >97%; i-C_4H_9I, >97%; t-C_4H_9I, >95%; 1-$C_5H_{11}I$, >98%; 1-$C_6H_{13}I$, >98%). All reagents (alkyl iodides) were purified by trap-to-trap distillation. Ar was purified by passing through a cold trap (−140 °C). Indicated error limits for the experimental results are at two standard deviations level throughout the paper.

Results

A. Thermal Decomposition of C_3−C_4 Alkyl Radicals. Figure 1a shows the observed time profiles of I- and H-atom concentrations in the thermal decomposition of n-C_3H_7I. The observed concentration of H atoms was much smaller than that of I atoms, which is a measure of the initial concentration of n-C_3H_7 radicals, indicating that the thermal decomposition of n-C_3H_7 produces little H atoms. On the other hand, as shown

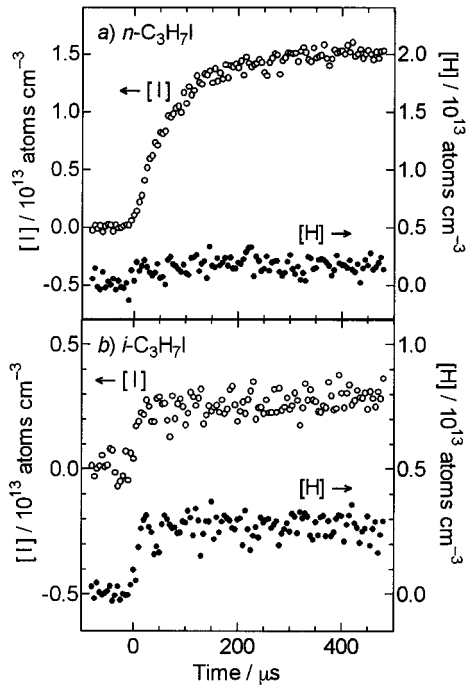

Figure 1. Observed time profiles of I- and H-atom concentrations in the thermal decomposition of (a) n-C_3H_7I and (b) i-C_3H_7I. Experimental conditions for (a): [I-atom trace] T = 1039 K, P = 0.99 atm, 3 ppm n-C_3H_7I/Ar; [H-atom trace] T = 1033 K, P = 0.99 atm, 15-ppm n-C_3H_7I/Ar. Note that the scales for [I] and [H] are shifted for clarity and that the initial concentration of n-C_3H_7I is 5 times grater in the H-atom measurement than in the I-atom measurement. Experimental conditions for *b*): [I-atom trace] T = 1364 K, P = 1.17 atm, 1-ppm i-C_3H_7I/Ar; [H-atom trace] T = 1398 K, P = 1.23 atm, 1-ppm i-C_3H_7I/Ar.

in Figure 1b, the yield of H-atoms is almost unity in the thermal decomposition of i-C_3H_7 radicals. Since, in the thermal decomposition of i-C_3H_7I, the branching fraction for molecular elimination (1b) is large (0.6−0.8), significant decrease of H atoms and increase of I atoms were observed under high initial concentrations of i-C_3H_7I, due to the reaction

$$H + HI \rightarrow H_2 + I \quad (4)$$

In order to minimize the effect of this reaction, the initial concentration was kept low especially for i-C_3H_7I experiments, although this effect is still slightly visible in Figure 1b which was observed under the initial concentration as low as 1 ppm. For n-C_3H_7I, the branching fraction for HI elimination (1b) is smaller (0.2−0.3) and thus higher initial concentration was applied in order to confirm the very small yield of H atoms.

The H-atom yields from the thermal decomposition of two isomeric propyl radicals at different temperatures are summarized in Figure 2. The H-atom yield from the thermal decomposition of i-C_3H_7 radical was unity within the experimental error limit, 1.01 ± 0.27, and was found to be independent of temperature. This indicates the dominance of the C−H bond fission in the thermal decomposition of i-C_3H_7 radical,

$$i\text{-}C_3H_7 + M \rightarrow C_3H_6 + H + M$$

$$\Delta H_{298} = 35.7 \text{ kcal mol}^{-1} \quad (5)$$

This is the only possible reaction channel except for the isomerization to n-C_3H_7. The H-atom yield from n-C_3H_7 radical was found to be much smaller, <0.05. This result indicates the dominance of the energetically favored C−C bond cleavage (6a)

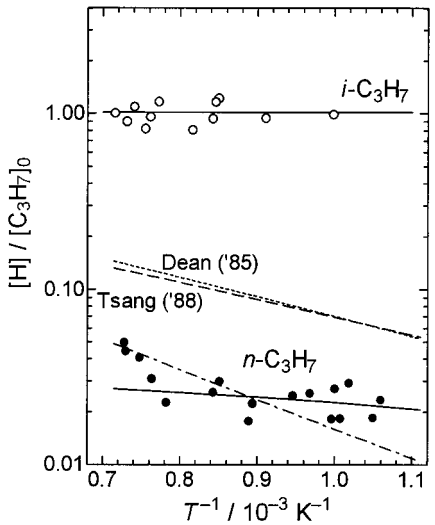

Figure 2. H-atom yield (=[H]/[C_3H_7]$_0$) from the thermal decomposition of *n*-C_3H_7 (●) and *i*-C_3H_7 (○) radicals. Solid line (—) through *i*-C_3H_7 data (○) denotes the averaged H-atom yield from *i*-C_3H_7. Solid line (—) and dotted broken line (— - - - —) through *n*-C_3H_7 data (●) denote the results of RRKM-fit and high-pressure limit fit, respectively (see text for detail). Dotted line (- - -) and broken line (— — —) denote the high-pressure limit estimates by Dean[3] and by Tsang,[4] respectively. Experimental conditions: [*n*-C_3H_7 (●)] P = 1.0−1.4 atm, 12−15 ppm *n*-C_3H_7I/Ar; [*i*-C_3H_7 (○)] P = 1.0−1.2 atm, 1-ppm *i*-C_3H_7I/Ar.

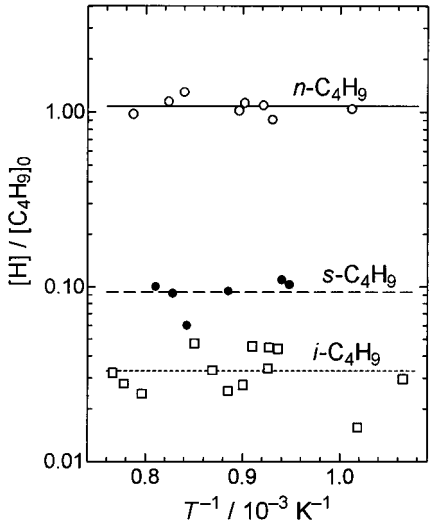

Figure 3. H-atom yield (=[H]/[C_4H_9]$_0$) from the thermal decomposition of *n*-C_4H_9 (○), *s*-C_4H_9 (●), and *i*-C_4H_9 (□) radicals. Lines through experimental data points are the averaged H-atom yields. Experimental conditions: [*n*-C_4H_9 (○)] P = 1.0−1.1 atm, [*s*-C_4H_9 (●)] P = 0.9−1.0 atm, [*i*-C_4H_9 (□)] P = 0.7−1.1 atm. Sample gas concentration was 1−10 ppm.

over C−H bond cleavage (6b) in this temperature range (1000−1400 K)

$$n\text{-}C_3H_7 + M \rightarrow C_2H_4 + CH_3 + M \qquad \Delta H_{298} = 23.3 \text{ kcal mol}^{-1} \quad (6a)$$

$$\rightarrow C_3H_6 + H + M \qquad \Delta H_{298} = 32.9 \text{ kcal mol}^{-1} \quad (6b)$$

The observed very small H-atom yield, 0.03−0.05, should be treated with care since, considering the purity of *n*-C_3H_7I reagent used (<97%), a small impurity (<3%; possibly, other alkyl iodides) might be the main source of the observed H atoms. The true branching fraction for (6b) may be even smaller. No apparent pressure dependence of the H-atom yield was found for either *n*-C_3H_7 or *i*-C_3H_7 in the pressure range 1.0−1.4 or 1.0−1.2 atm, respectively.

The observed H-atom yield from the butyl radicals *n*-C_4H_9, *s*-C_4H_9, and *i*-C_4H_9 are summarized in Figure 3. The H-atom yield from the thermal decomposition of *n*-C_4H_9 radicals was unity within the experimental error limit (1.08 ± 0.24). This does not imply the dominance of C−H bond fission (7b) since C_2H_5 radical formed by C−C rupture (7a) successively decomposes to C_2H_4 + H (3)

$$n\text{-}C_4H_9 + M \rightarrow C_2H_4 + C_2H_5 + M \qquad \Delta H_{298} = 22.4 \text{ kcal mol}^{-1} \quad (7a)$$

$$\rightarrow 1\text{-}C_4H_8 + H + M \qquad \Delta H_{298} = 33.1 \text{ kcal mol}^{-1} \quad (7b)$$

Although the observation of H atoms could tell nothing on the branching fractions for (7a) and (7b), the main dissociation channel is expected to be the C−C rupture (7a) from the results for *n*-C_3H_7 as well as those for *s*-C_4H_9 and *i*-C_4H_9, which will be shown below.

The small H-atom yields for *s*-C_4H_9 (∼0.09) and *i*-C_4H_9 (∼0.03) indicate the dominance of C−C bond cleavage ((8a) and (9a)) in the thermal decomposition of *s*-C_4H_9 and *i*-C_4H_9 radicals

$$s\text{-}C_4H_9 + M \rightarrow C_3H_6 + CH_3 + M \qquad \Delta H_{298} = 23.9 \text{ kcal mol}^{-1} \quad (8a)$$

$$\rightarrow 1\text{-}C_4H_8 + H + M \qquad \Delta H_{298} = 36.2 \text{ kcal mol}^{-1} \quad (8b)$$

$$\rightarrow 2\text{-}C_4H_8 + H + M \qquad \Delta H_{298} = 33.7 \text{ kcal mol}^{-1} \quad (8c)$$

$$i\text{-}C_4H_9 + M \rightarrow C_3H_6 + CH_3 + M \qquad \Delta H_{298} = 22.9 \text{ kcal mol}^{-1} \quad (9a)$$

$$\rightarrow i\text{-}C_4H_8 + H + M \qquad \Delta H_{298} = 31.3 \text{ kcal mol}^{-1} \quad (9b)$$

For the reasons similar to *n*-C_3H_7, these small H-atom yield should be discussed carefully. Especially for *s*-C_4H_9I, since the branching fraction for C−I bond fission (1a) is small (∼0.2), small (∼3%) impurity in the *s*-C_4H_9I reagent might produce the H atoms corresponding to the H-atom yield as high as ∼15%. For this reason, the H-atom yield of ∼0.09, which seems significantly large, may be solely ascribed to the impurity. No apparent pressure dependence of the H-atom yield was found for either butyl radical in the pressure range 0.7−1.1 atm. A trial was also made to investigate the H-atom yield from *t*-C_4H_9 radical,

$$t\text{-}C_4H_9 + M \rightarrow i\text{-}C_4H_8 + H + M \qquad (10)$$

by the thermal decomposition of *t*-C_4H_9I. However, for this iodide, the molecular elimination process (1b) is almost exclusively dominant and almost no I atoms were observed (<0.05). Since this extremely small I-atom yield (<0.03) may be attributed to the impurity, *t*-C_4H_9I could not be used as the

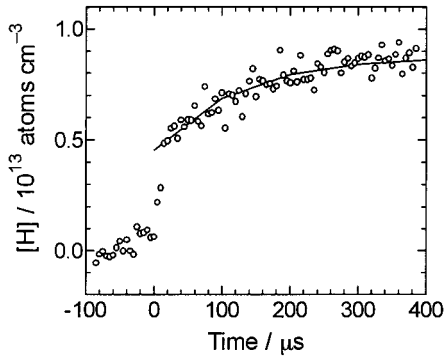

Figure 4. Observed time profile of H-atom concentration in the thermal decomposition of 1-$C_5H_{11}I$. Experimental conditions: $T = 1200$ K, $P = 1.0$ atm, 4-ppm 1-$C_5H_{11}I$/Ar. The solid line represents the result of the numerical simulation (see text).

precursor for *t*-C_4H_9 radicals. The I-atom yield was found to be high (0.6∼0.9) for primary iodides while it was smaller (0.2−0.4) for secondary iodides, and further smaller for the tertiary one (<0.05) which has been discussed in the previous work.[15]

All the results for C_3-C_4 alkyl radicals indicate the dominance of the C−C bond fission channel in the present experimental conditions (900−1400 K, ∼1 atm) except for the result for *n*-C_4H_9 which is, however, also consistent with this conclusion.

B. Isomerization Processes of Alkyl Radicals. The present distinct results between *n*-C_3H_7 and *i*-C_3H_7 radicals imply the insignificance of the three-membered ring 1,2 primary-to-secondary (3sp) or the reverse 2,1 secondary-to-primary (3ps) isomerization reaction,

$$n\text{-}C_3H_7 + M \leftrightarrow i\text{-}C_3H_7 + M \qquad (6c)$$

Although a lower activation energy is expected for 1,2 primary-to-tertiary (3tp) isomerization, the very small H-atom yield (∼0.03) observed for *i*-C_4H_9 implies the minority of 3tp isomerization

$$i\text{-}C_4H_9 + M \rightarrow t\text{-}C_4H_9 + M \qquad (9c)$$

since *t*-C_4H_9 is expected to decompose predominantly to *i*-C_4H_8 + H (10). Similarly, the results for *n*-C_4H_9 and *s*-C_4H_9 also imply the insignificance of four-membered ring 1,3 primary-to-secondary (4sp) or 3,1 secondary-to-primary (4ps) isomerization reaction

$$n\text{-}C_4H_9 + M \leftrightarrow s\text{-}C_4H_9 + M \qquad (7c)$$

These results are consistent with the previous indications[8,11g,h] that the threshold energy for three- or four-membered ring isomerization is higher than that for C−H fission (∼34 kcal mol^{-1}) and the expected smaller *A* factors, which will be discussed later. In order to investigate the possibility of isomerization reactions via larger ring transition state, experiments were extended to 1-C_5H_{11} and 1-C_6H_{13} radicals.

Figure 4 shows a typical time profile of H-atom concentration observed in the thermal decomposition of 1-$C_5H_{11}I$. The rapid H-atom formation is ascribed to the thermal decomposition of 1-C_5H_{11} while the slower part is ascribed to a side reaction, thermal decomposition of 1-C_5H_{10} (1-pentene) produced by the HI elimination (branching fraction is ∼0.54) from 1-$C_5H_{11}I$. Since the allylic C−C bond in 1-C_5H_{10} is weak, its thermal decomposition

$$1\text{-}C_5H_{10} + M \rightarrow C_3H_5 + C_2H_5 + M \qquad (11)$$

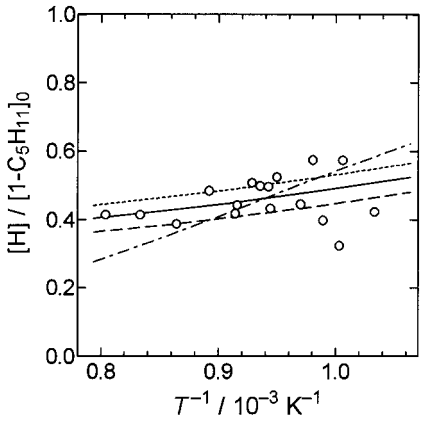

Figure 5. H-atom yield (=[H]/[1-$C_5H_{11}]_0$) from the thermal decomposition of 1-C_5H_{11} radical. Dotted broken line (− - − - −) denotes the result of high-pressure limit fit (see text). The three parallel lines represent the results of RRKM calculations with different threshold energies for five-membered ring primary-to-secondary isomerization [E_0(5sp)]; E_0(5sp) = 20.2 (- - -), 20.5 (− − −), and 20.8 (- − -) kcal mol^{-1} (see text). Experimental conditions: $P = 0.7-1.2$ atm, 4-ppm 1-$C_5H_{11}I$/Ar.

is relatively fast and the subsequent decomposition of C_2H_5 (3) or C_3H_5(allyl radical)

$$C_3H_5(\text{allyl}) + M \rightarrow C_3H_4(\text{allene}) + H + M \qquad (12)$$

produces hydrogen atoms. The slower part of the H-atom formation was observed above ∼1100 K, which is consistent with the reported rate constants[16] for the thermal decomposition of 1-pentene. The solid line in Figure 4 shows the numerical simulation using the rate constant for reaction 11, 3.6×10^3 s^{-1}, which is slightly larger than the previously reports.[18] The fast rise of the H-atom formation could be clearly separated from the slow rise up to ∼1250 K. The evaluated H-atom yield from the thermal decomposition of 1-C_5H_{11} radical is summarized in Figure 5.

Similar slow production of hydrogen atoms was also observed in the thermal decomposition of 1-$C_6H_{13}I$, which was ascribed to the thermal decomposition of 1-C_6H_{12} (1-hexene)

$$1\text{-}C_6H_{12} + M \rightarrow C_3H_5 + n\text{-}C_3H_7 + M \qquad (13)$$

formed by the HI elimination (branching fraction is ∼0.47) from 1-$C_6H_{13}I$, and the subsequent H-atom formation via reaction 12. The H-atom yield from the thermal decomposition of 1-C_6H_{13} radical could be separated from the slow H-atom production by the side reaction up to ∼1300 K, and is plotted in Figure 6.

For the thermal decomposition of 1-C_5H_{11}, possible reaction channels except for isomerization are

$$1\text{-}C_5H_{11} + M \rightarrow C_2H_4 + n\text{-}C_3H_7 + M \qquad \Delta H_{298} = 22.7 \text{ kcal mol}^{-1} \qquad (14a)$$

$$\rightarrow 1\text{-}C_5H_{10} + H + M \qquad \Delta H_{298} = 33.1 \text{ kcal mol}^{-1} \qquad (14b)$$

Since, as shown above, C−C bond cleavage is generally preferred to C−H cleavage for C_3-C_4 alkyl radicals and the heats of reaction for (14a) and (14b) are quite similar to those for C−C and C−H fission reactions of C_3-C_4 radicals, the branching fraction for (14b) is expected to be negligibly small. However, as shown in Figure 5, the H-atom yield from 1-C_5H_{11}

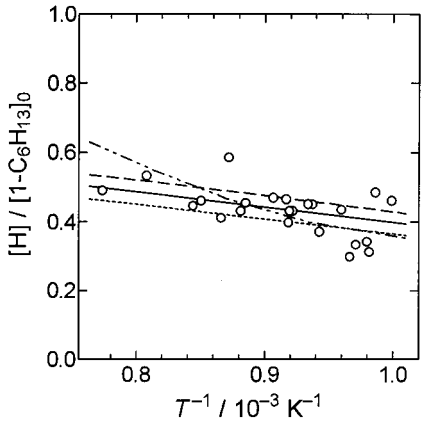

Figure 6. H-atom yield (=[H]/[1-C_6H_{13}]$_0$) from the thermal decomposition of 1-C_6H_{13} radical. Dotted broken line (− - − - −) denotes the result of high-pressure limit fit (see text). The three parallel lines represent the results of RRKM calculations with different threshold energies for five-membered ring primary-to-secondary isomerization [E_0(6sp)]; E_0(6sp) = 14.3 (- - -), 14.6 (− − −), and 14.9 (- − -) kcal mol^{-1} (see text). Experimental conditions: P = 0.8−1.2 atm, 4-ppm 1-C_6H_{13}I/Ar.

radical is quite large, 0.4−0.5. This result indicates the occurrence of the five-membered ring 1,4 primary-to-secondary (5sp) isomerization

$$1\text{-}C_5H_{11} + M \rightarrow 2\text{-}C_5H_{11} + M \qquad (14c)$$

followed by the thermal decomposition of 2-C_5H_{11}

$$2\text{-}C_5H_{11} + M \rightarrow C_3H_6 + C_2H_5 + M \qquad (15)$$

and subsequent decomposition of C_2H_5 to C_2H_4 + H (3).

For the case of 1-C_6H_{13}, both of the possible direct dissociation channels

$$1\text{-}C_6H_{13} + M \rightarrow C_2H_4 + n\text{-}C_4H_9 + M \qquad (16a)$$

$$\rightarrow 1\text{-}C_6H_{12} + H + M \qquad (16b)$$

expected to produce one H atom since the subsequent dissociation of n-C_4H_9 quantitatively produces H atom as shown before. However, the observed H-atom yield was clearly less than unity, 0.4−0.5 (Figure 6). Accordingly, this result should be ascribed to the six-membered ring 1,5 primary-to-secondary (6sp) isomerization reaction,

$$1\text{-}C_6H_{13} + M \rightarrow 2\text{-}C_6H_{13} + M \qquad (16c)$$

The resultant 2-C_6H_{13} radical is expected to produce few H atoms via the reaction

$$2\text{-}C_6H_{13} + M \rightarrow C_3H_6 + n\text{-}C_3H_7 + M \qquad (17)$$

followed by the decomposition of n-C_3H_7 dominantly to C_2H_4 + CH_3 (6a).

Discussion

A. Falloff Effect to the Branching Fraction for n-C_3H_7. The present experimental results for C_3 and C_4 alkyl radicals indicate the dominance of C−C bond cleavage in the thermal decomposition processes. The branching fractions for the competitive C−H bond fission channels were below the detection limits imposed by the impurities in the reagents.

As a preliminary analysis for the two-channel thermal decomposition of n-C_3H_7, a transition state theory (TST) calculation, that is an RRKM calculation in the high-pressure limit, was performed. Geometry and vibrational frequencies of the reactant and the transition states (TS's) were estimated by Hartree−Fock level [HF/6-31G(d)] ab initio calculations by using Gaussian 94.[17] The frequencies were scaled by 0.8929, which is the recommended scale factor for HF/6-31G(d).[18] One C_2H_5−$CH_2^\bullet$ torsion motion of n-C_3H_7 and one C_2H_4−CH_3 torsion of the C−C fission TS were treated as free rotors. The threshold energy for the C−C fission channel was fixed to 29.5 kcal mol^{-1}, which has been derived by Bencsura et al.[1b] The result of this high-pressure limit fit to the observed branching fraction is shown in Figure 2 by a dotted broken line (− - − - −), where only the threshold energy for higher C−H fission channel, E_0(C−H), was adjusted so as to reproduce the experimental branching fraction. As the best fit, E_0(C−H) was derived to be 36.5 kcal mol^{-1}. Since the observed branching fraction should be treated as the upper limit as described above, the high-pressure limit calculation suggests that E_0(C−H) ≥ 36.5 kcal mol^{-1}. From the thermochemical data,[19] this corresponds to the threshold energy for the reverse reaction, ≥4.7 kcal mol^{-1}, which is apparently too large in comparison with E_0 = 2.2 kcal mol^{-1} for C_2H_4 + H[1c] or the generally suggested activation energy, E_a = 2.5 kcal mol^{-1}, for primary radical formation.[3] This discrepancy could not be explained by the uncertainty of the preexponential factors (about ±30%) due to the errors in the estimated geometry and frequencies.

Also, previous estimates[3,4] for the high-pressure limit predicted larger branching fractions for C−H rupture (6b), 0.10−0.11, than the present result, <0.04, at 1200 K as shown in Figure 2. No significant error in the previous estimations could be found since they are based on the thermochemistry and the rather certain rate parameters for reverse reactions which have been measured at lower temperatures, and where the high-pressure limit was easily fulfilled. This discrepancy and the failure of the high-pressure limit fit imply that the present experimental conditions did not satisfy the complete high-pressure limiting condition. In order to investigate the falloff effect to the branching fraction, two-channel RRKM calculation was performed for n-C_3H_7. The calculation was carried out by using UNIMOL program suit.[20] The solution of the master equation was obtained by solving the eigenvalue problem in the form,[21]

$$\mathbf{Mg} = -k_{tot}\mathbf{g} \qquad (18)$$

where **g** is the steady-state population distribution, k_{tot} is the overall rate constant, and **M** is a matrix consists of energy transfer rate constants and microscopic reaction rate constants. An exponential down model[23] with α = 500 cm^{-1} was assumed for the energy transfer probabilities. The microcanonical rate constant at energy E was calculated by the RRKM formula, $k(E) = [n^\ddagger\sigma/n\sigma^\ddagger][Q_R^\ddagger/Q_R][W^\ddagger(E-E_0)/h\rho(E)]$,[23] where n, σ, Q_R, $n^\ddagger$, $\sigma^\ddagger$, and $Q_R^\ddagger$ denote the number of optical isomers and rotational conformers, rotational symmetry number, and rotational partition function of the reactant, and those for the TS, respectively. $W^\ddagger$ and ρ denote the sum of states of the TS and the density of states of the reactant, respectively, and h is the Planck constant. The geometry and the frequencies of reactant and TS's and the threshold energy for C−C fission were the same as those used in the TST calculation described above.

In the RRKM fit, similarly to the TST fit, only E_0(C−H) was adjusted so as to reproduce the observed branching fraction. The best fit to the experimental branching fraction (a solid line through solid circles in Figure 2) was found at E_0(C−H) = 33.5 kcal mol^{-1} and hence the RRKM fit suggests E_0(C−H) ≥ 33.5

kcal mol^{-1}. The corresponding E_0 for the reverse reaction, $\geq$1.7 kcal mol^{-1}, is in reasonable comparison with E_0 = 2.2 kcal mol^{-1} or E_a = 2.5 kcal mol^{-1} described above. Further, the high-pressure limit calculation with this E_0(C−H) gave the branching fraction close to the previous estimates[3,4] (coinciding with the broken line in Figure 2). These analyses show the importance of the falloff effect especially in the branching fraction for multichannel dissociation processes because the population depletion by the lower channel enhances the falloff effect for the higher channel. The RRKM calculation predicts that the branching fraction for C−H fission even at 10 atm ($\sim$0.044) is still far less than the high-pressure limit ($\sim$0.10) at 1200 K, where the overall rate constant is fairly close to the high-pressure limit, that is, k(10 atm)/k^∞ = 0.13. In the above analysis, the average downward energy transferred per collision, $\langle\Delta E_{down}\rangle$, was set to be 500 cm^{-1}, which is a typical value for relatively large organic molecules,[22] and was assumed to be independent of temperature. The derived threshold energy is not so sensitive to this quantity. For example, a change of $\langle\Delta E_{down}\rangle$ by $\pm$200 cm^{-1} changed the best fit E_0(C−H) by only $\pm$0.3 kcal mol^{-1}.

B. Analysis of the Competition between Isomerization and Dissociation. The present results for 1-C_5H_{11} and 1-C_6H_{13} radicals indicate the occurrence of five- and six-membered ring primary-to-secondary (5sp and 6sp) isomerization reactions. As a rough high-pressure limit picture, the present results indicate that the isomerization proceeds with a rate nearly equal to the direct C−C fission, and thus, the activation energy for the isomerization should be significantly lower than that for the C−C fission since a lower preexponential factor is expected for the isomerization via ring TS.[8] However, the observed temperature dependence of the H-atom yield was very small and contradicts the expected large difference of activation energy. This implies the breakdown of the high-pressure limit assumption, which will be shown below more quantitatively.

The procedure used in the high-pressure limit TST analysis is similar to that for n-C_3H_7 described in the previous subsection. Only the threshold energies for the isomerization processes were adjusted so as to reproduce the observed H-atom yield. The minor C−H fission processes and three- or four-membered ring isomerization processes were ignored, and only the C−C fission processes and five- and six-membered ring isomerization processes were considered. The estimated energy diagrams for these processes are shown in Figure 7. Threshold energies for the C−C fission processes were estimated to be ΔH_0 + 7.7 kcal mol^{-1} from the reported[1] threshold energies for smaller alkyl radicals, which is also in good comparison with E_a = ΔH_{300} + 7 kcal mol^{-1} suggested[3] generally for the C−C fission reactions of alkyl radicals. The threshold energy for 5sp isomerization of 1-C_6H_{13} was assumed to be the same as that for 1-C_5H_{11}. The threshold energy for 5sp isomerization, E_0(5sp), was derived from the best fit to the 1-C_5H_{11} data (Figure 5) and, by using this, the threshold energy for 6sp isomerization, E_0(6sp), was derived from the best fit to the 1-C_6H_{13} data (Figure 6). By including the effects of the backward isomerization processes from 2-C_5H_{11} to 1-C_5H_{11} and from 2- or 3-C_6H_{13} to 1-C_6H_{13}, the observed H-atom yields can be related to the branching fractions for individual processes as

$$\frac{[\mathrm{H}]}{[1\text{-}\mathrm{C_5H_{11}}]_0} = \frac{f_{1\mathrm{p},1} f_{2\mathrm{p},2}}{1 - f_{1\mathrm{p},1} f_{2\mathrm{p},1}} \tag{19}$$

$$\frac{[\mathrm{H}]}{[1\text{-}\mathrm{C_6H_{13}}]_0} = \frac{f_{1\mathrm{h},3} + f_{1h,2} f_{3\mathrm{h},2}}{1 - f_{1\mathrm{h},1} f_{2\mathrm{h},1} - f_{1\mathrm{h},2} f_{3\mathrm{h},1}} \tag{20}$$

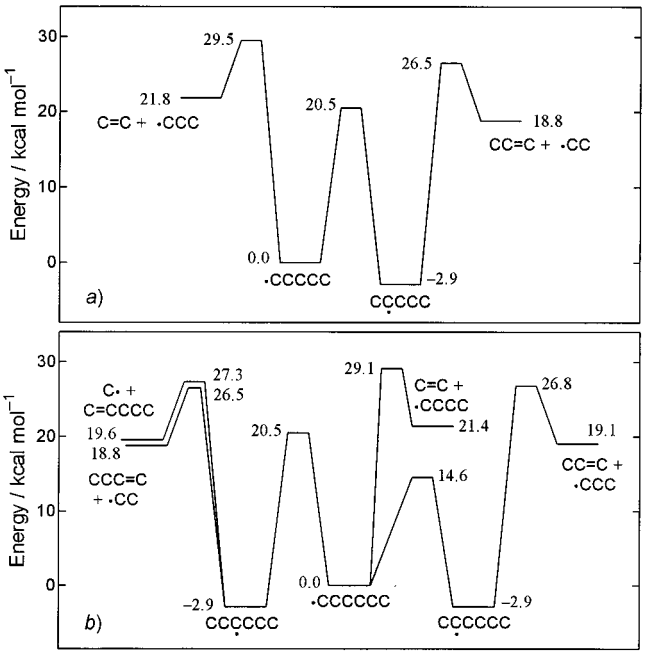

Figure 7. Estimated energy diagrams for dissociation and isomerization processes of (a) 1-C_5H_{11} and (b) 1-C_6H_{13} radicals. The ordinate is relative enthalpies at 0 K.

where $f_{1\mathrm{p},i}$ and $f_{2\mathrm{p},i}$ denote the branching fractions for 1- and 2-pentyl(C_5H_{11}) radicals, respectively, numbered (i) in the order from lower to upper channels; that is, i = 1 denotes the isomerization process and i = 2 denotes the C−C fission process (see Figure 7a). Similarly, $f_{1\mathrm{h},i}$, $f_{2\mathrm{h},i}$, and $f_{3\mathrm{h},i}$ denote the branching fractions for 1-, 2-, and 3-hexyl(C_6H_{13}), respectively. Also i is the channel number from lower to upper (see Figure 7b).

The results of the TST-fit are shown in Figures 5 and 6 by dotted broken lines (− - − - −). As expected, this high-pressure limit analysis could not reproduce the observed small temperature dependence of the H-atom yields, and the falloff effect is implied to be important even for these large alkyl radicals. The derived threshold energies for the isomerization processes; E_0(5sp) = 17.8 and E_0(6sp) = 9.8 kcal mol^{-1}, were apparently too low in comparison with the previous results and theoretical investigations which will be shown below.

For the quantitative analysis of the falloff effect, multichannel RRKM calculations were also performed for C_5H_{11} and C_6H_{13} systems. By assuming the independent steady-state distribution for each isomer, the rate constants can be derived from the independent eigenvalue problems similar to eq 18,

$$\begin{aligned}
\mathbf{M}_{1\mathrm{p}}\mathbf{g}_{1\mathrm{p}} &= -k_{1\mathrm{p}}\mathbf{g}_{1\mathrm{p}} \\
\mathbf{M}_{2\mathrm{p}}\mathbf{g}_{2\mathrm{p}} &= -k_{2\mathrm{p}}\mathbf{g}_{2\mathrm{p}} \qquad (21) \\
\mathbf{M}_{1\mathrm{h}}\mathbf{g}_{1\mathrm{h}} &= -k_{1\mathrm{h}}\mathbf{g}_{1\mathrm{h}} \\
\mathbf{M}_{2\mathrm{h}}\mathbf{g}_{2\mathrm{h}} &= -k_{2\mathrm{h}}\mathbf{g}_{2\mathrm{h}} \\
\mathbf{M}_{3\mathrm{h}}\mathbf{g}_{3\mathrm{h}} &= -k_{3\mathrm{h}}\mathbf{g}_{3\mathrm{h}} \qquad (22)
\end{aligned}$$

where suffixes 1p, 2p, 1h, 2h, and 3h denote the properties for 1-, 2-pentyl (C_5H_{11}), 1-, 2-, and 3-hexyl (C_6H_{13}), respectively. The observed H-atom yields can be related to the branching fractions in the same manner as the TST calculation by eqs 19 and 20. This analysis will be referred as *independent* treatment hereinafter.

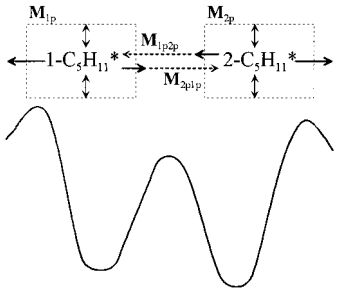

Figure 8. Schematic representation of the *simultaneous* treatment for pentyl (C_5H_{11}) system. $\mathbf{M}_{1p}$, $\mathbf{M}_{2p}$, $\mathbf{M}_{1p2p}$, and $\mathbf{M}_{2p1p}$ indicate the microcanonical processes described by the corresponding matrices in eq 23 (see text for detail).

The above assumption of the independent steady-state for the each isomer may not be valid at high temperatures. For example, for the pentyl (C_5H_{11}) case, the fast isomerization from 1-C_5H_{11} to 2-C_5H_{11} interferes with the steady-state distribution of 2-C_5H_{11} and, also, the reverse isomerization interferes that of 1-C_5H_{11}. In order to treat this problem properly, a different type of RRKM calculation was also performed by solving the problem represented by,

$$\begin{pmatrix} \mathbf{M}_{1p} & \mathbf{M}_{1p2p} \\ \mathbf{M}_{2p1p} & \mathbf{M}_{2p} \end{pmatrix} \begin{pmatrix} \mathbf{g}_{1p} \\ \mathbf{g}_{2p} \end{pmatrix} = -k_{1p} \begin{pmatrix} \mathbf{g}_{1p} \\ \mathbf{0} \end{pmatrix} \tag{23}$$

$$\begin{pmatrix} \mathbf{M}_{1h} & \mathbf{M}_{1h2h} & \mathbf{M}_{1h3h} \\ \mathbf{M}_{2h1h} & \mathbf{M}_{2h} & \mathbf{0} \\ \mathbf{M}_{3h1h} & \mathbf{0} & \mathbf{M}_{3h} \end{pmatrix} \begin{pmatrix} \mathbf{g}_{1h} \\ \mathbf{g}_{2h} \\ \mathbf{g}_{3h} \end{pmatrix} = -k_{1h} \begin{pmatrix} \mathbf{g}_{1h} \\ \mathbf{0} \\ \mathbf{0} \end{pmatrix} \tag{24}$$

where suffixes such as 1p2p denote the cross term; for example, 1p2p denotes the effect of the distribution in 2-pentyl to 1-pentyl. The cross term matrices such as $\mathbf{M}_{1p2p}$ are diagonal and consist of microscopic rate constants only. A schematic representation of this treatment (which will be referred as *simultaneous* treatment hereinafter) is shown in Figure 8 for the pentyl (C_5H_{11}) case. The cross terms, $\mathbf{M}_{1p2p}$ and $\mathbf{M}_{2p1p}$, represent the population interference between the two isomers, which is neglected in the independent treatment. For the hexyl (C_6H_{13}) case, the cross terms between 2-hexyl and 3-hexyl are null since no isomerization between these two was considered (eq 24). It should be noted that the right-hand side of eq 23 or 24 is *not* ${}^{T}(\mathbf{g}_{1p}, \mathbf{g}_{2p})$ or ${}^{T}(\mathbf{g}_{1h}, \mathbf{g}_{2h}, \mathbf{g}_{3h})$ since, for example by the 1-C_5H_{11} case, the problem to be solved is the steady-state dissociation of 1-pentyl radical, but not the steady-state dissociation of the mixture of 1- and 2-pentyl. The solution of eq 23 or 24 was obtained numerically by iteration starting from a initial guess of the population distribution.

The geometry, frequencies, and threshold energy for C−C fission processes were the same as those used in the TST calculations. The average downward energy transferred per collision, $\langle \Delta E_{down} \rangle$, was assumed to be 500 cm^{-1} and independent of temperature. In the RRKM fit, similarly to the TST fit described above, the threshold energy for 5sp isomerization of 1-C_6H_{13} was assumed to be the same as that for 1-C_5H_{11} and thus E_0(5sp) was derived from the best fit to the 1-C_5H_{11} data and E_0(6sp) was derived from the best fit to the 1-C_6H_{13} data. The results of the RRKM fit with independent treatment are shown in Figures 5 and 6 by solid lines. The derived threshold energies were E_0(5sp) = 20.5 and E_0(6sp) = 14.6 kcal mol^{-1}. The RRKM calculation well reproduces the observed small temperature dependence of the H-atom yields. The simultaneous treatment shows quite different population distribution, and thus different rate constants for each process, from the independent treatment, as shown in Figure 9. The simultaneous treatment predicts lower total steady-state concentration in 2-pentyl and, as expected, the hotter energy distribution in 2-pentyl than the independent treatment. However, these differences did not affect the calculated H-atom yields so much. The calculated difference in the H-atom yields between these two treatments was only <0.0025 for 1-C_5H_{11} and <0.0060 for 1-C_6H_{13}, and thus the best fit threshold energies were unchanged from the results of the independent treatment, that is E_0(5sp) = 20.5 and E_0(6sp) = 14.6 kcal mol^{-1}. The error limit of the threshold energies was estimated to be ±1.2 kcal mol^{-1} by considering the possible errors from the data scattering, errors in the H-atom calibration, the uncertainty of the estimated threshold energies for C−C fission channels, and the uncertainty of the value of the $\langle \Delta E_{down} \rangle$ (assumed to be ±200 cm^{-1}).

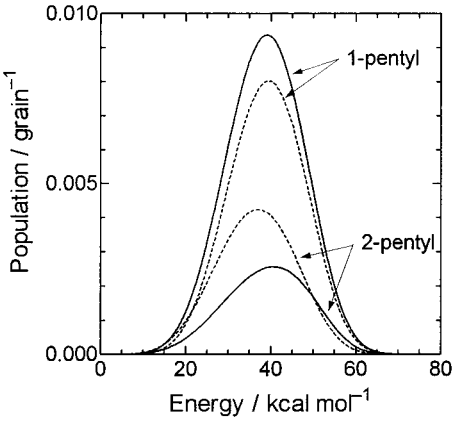

Figure 9. Comparison of the steady-state internal population distributions of pentyl (C_5H_{11}) radicals calculated with independent (- - -) and simultaneous (— — —) treatments at 1260 K and 1 atm (see text for details). The abscissa indicates the energy from the ground state of the 2-pentyl radical. The ordinate is the population per grain (the grain size is 100 cm^{-1}) and the distribution has been normalized so that the sum of the populations in 1- and 2-pentyl is unity. The calculations were performed with E_0(5sp) = 20.5 kcal mol^{-1}.

Although no significant difference was found in the calculated H-atom yield, the difference of the calculated population distributions between the two treatments (Figure 9) indicates that the mutual effect of the population distribution is essentially important. For example, the dissociation rate constant for 2-pentyl calculated by the simultaneous treatment is about 2 times larger than that calculated by the independent treatment. In the case of the dissociation starting from the primary radical side as the present experiments (from 1-C_5H_{11} or 1-C_6H_{13}), the contribution of the backward isomerization is minor and the effect on the branching fraction was small. However, the dissociation from the secondary radical side may show larger effect than the present case. This problem should be investigated in further experimental and theoretical studies.

C. Nonequilibrium Effect in the Branching Fractions. The deviation of the population distribution of 2-pentyl from the independent steady state as shown in Figure 9 is a similar problem to those called nonequilibrium or non-steady-state effect,[23,24] and to the chemical activation reactions.[10,25] In the above RRKM analysis, such an effect was considered in only the isomerization product radicals. However, as pointed out by Tsang et al.,[26] the nonequilibrium effect may be important generally in the radical species (with low dissociation thresholds) generated in the high-temperature chain reaction. In order to assess this effect in the present experiments as well as in the practical combustion conditions, a discussion will be done below.

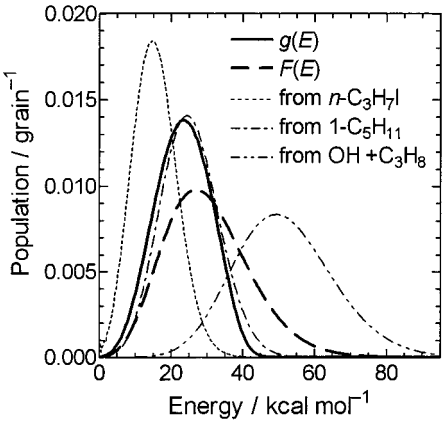

Figure 10. Comparison of the estimated nascent population distributions of n-C_3H_7 produced by n-C_3H_7I + M (- - -), 1-C_5H_{11} + M (− - − - −), and OH + C_3H_8 (− - - − - - −) at 1400 K and 1.1 atm (Ar). The ordinate is the population per grain (the grain size is 100 cm^{-1}) and the distributions have been normalized. The steady-state distribution calculated by eq 18, $g(E)$ (—), and the Boltzmann distribution, $F(E)$ (− − −), are also shown for comparison.

The nonequilibrium effect has been investigated[25,26] by the time-dependent solution of the master equation starting from the thermal Boltzmann distribution at the bath-gas temperature. However, the "initial distribution" in the actual reaction system will be more complicated and different from the Boltzmann distribution. The nascent internal energy distribution should apparently depend on the kind of reaction process that produces the radical of interest. The highly exothermic reaction with significant barrier, such as OH + alkane, will produce highly excited radicals while the endothermic reaction without barrier, such as C−C bond fission of alkane, will produce radicals with less excess energy. Here, as an example, nonequilibrium RRKM calculations on the two-channel dissociation of n-C_3H_7 radical produced by three types of reactions

$$n\text{-}C_3H_7I + M \rightarrow I + n\text{-}C_3H_7 + M \qquad \text{(R1)}$$

$$1\text{-}C_5H_{11} + M \rightarrow C_2H_4 + n\text{-}C_3H_7 + M \qquad \text{(R2)}$$

$$OH + C_3H_8 \rightarrow H_2O + n\text{-}C_3H_7 \qquad \text{(R3)}$$

will be shown.

The nascent population distributions of the n-C_3H_7 radicals produced by (R1)−(R3) were estimated based on the prior distribution.[26] Details of the estimation procedure are described in the Appendix. The estimated nascent distribution of n-C_3H_7 produced by reactions R1−R3, the steady-state distribution calculated by eq 18 [$g(E)$], and the Boltzmann distribution [$F(E)$] are compared in Figure 10 [calculated at 1400 K and 1.1 atm (Ar)]. Very cool distribution was calculated for the barrierless simple C−I bond fission reaction (R1), while hotter distribution close to $g(E)$ was estimated for the C−C fission reaction (R2) with a pronounced barrier, that is, with 7.7 kcal mol^{-1} energy release from TS to products. The hottest distribution was calculated for the abstraction reaction (R3) because of the large exothermicity, $\Delta H_0 = -18.4$ kcal mol^{-1} (with a small barrier for this reaction, $E_0 \sim 1.3$ kcal mol^{-1}, totally 19.7 kcal mol^{-1} energy release is expected from TS to products). The rate constants and the branching fractions for these nonequilibrium conditions were calculated by solving the steady-state equation similar to the chemical activation problems,[27]

$$d\mathbf{g}/dt = \mathbf{Mg} + R\boldsymbol{\eta} = \mathbf{0} \qquad (25)$$

where $\mathbf{g}$ is the steady-state population distribution, R is the rate of formation of n-C_3H_7, and $\boldsymbol{\eta}$ is the incoming flux distribution, that is, the nascent population distribution of n-C_3H_7 such as those shown in Figure 10. This problem was solved by the inversion of the matrix,

$$\mathbf{g} = -R\mathbf{M}^{-1}\boldsymbol{\eta} \qquad (26)$$

In the actual calculation, the constant R was omitted since it does not affect the shape of the distribution $\mathbf{g}$. The calculation was made with the threshold energy for the C−C fission and the C−H fission of n-C_3H_7, 29.5 and 33.5 kcal mol^{-1}, which are the same as those used in the RRKM fit shown in Figure 2.

With cool distribution, $\boldsymbol{\eta}$ from (R1) or (R2), the calculated branching fractions for the C−H fission differ only very slightly (<0.0008) from the steady-state calculated by eq 18 at 1000−1400 K and 1.1 atm. However, with hot distribution from the OH reaction (R3), the calculated branching fraction for the C−H fission significantly [1.6 (1000 K) − 3.3 times (1400 K)] larger than the usual steady-state calculation at 1.1 atm.

The above calculations imply the importance of nonequilibrium effect in alkyl radical decomposition when it is generated by the highly exothermic reaction, such as H-abstraction reactions from alkanes. Since the H-abstraction reaction is one of the major sources of the alkyl radical, the nonequilibrium effect will be important in the practical combustion conditions. However, this effect is negligible in the present experiments, in which the alkyl radicals were generated from the barrierless decomposition of alkyl iodides. Similar calculations for 1-C_5H_{11} and 1-C_6H_{13} produced by the thermal decomposition of respective iodides showed that the nonequilibrium effect (except the one discussed as the "simultaneous treatment") is also negligible in the present experiments. It should be noted that the present calculations on the nonequilibrium effect were still rather qualitative since our experimental knowledge on the energy distribution in the reaction products is limited and the deviation from the prior distribution has been frequently reported in many reaction systems as "surprisal".[28]

D. Rate Parameters for Isomerization Reactions. Present experimental results showed the insignificance of the three- or four-membered ring isomerization processes. This is consistent with the high threshold energies estimated by ab initio calculation:[13b] $E_0(3sp) = 38.6$, $E_0(3tp) = 36.5$, and $E_0(4sp) = 38.1$ kcal mol^{-1}. Considering the lower threshold energies and larger preexponential factors (A factors) for C−C fission processes, three- or four-membered ring isomerization processes are hard to compete with C−C fission processes, but may compete with C−H fission processes in, for example, the thermal decomposition of t-C_4H_9 at extreme conditions. (See below for the general trend of the high-pressure limit rate parameters.)

From the RRKM fit to the present experiments for 1-C_5H_{11} and 1-C_6H_{13}, the threshold energies were derived as $E_0(5sp) = 20.5 \pm 1.2$ and $E_0(6sp) = 14.6 \pm 1.2$ kcal mol^{-1}. Recent ab initio calculation[13b] at MP−SAC2/6-311G(d,p) predicts $E_0(5sp) = 20.6-21.5$ kcal mol^{-1} and $E_0(6sp) = 13.4$ kcal mol^{-1} which are in good agreement with the present results.

The large difference between threshold energies for 5- and six-membered ring isomerization reactions can be interpreted mainly in terms of the ring-strain energy.[8] From the present result, the difference between the ring-strain energies between five- and six-membered ring transition state, $E_{RS}(5) - E_{RS}(6)$, was estimated to be 5.9 kcal mol^{-1}. Benson estimated that $E_{RS}(5) - E_{RS}(6) = 7$ kcal mol^{-1} based on the ring-strain energy of cycloalkanes, for which $E_{RS}(5) - E_{RS}(6) = 6.3$ kcal mol^{-1}. From the ab initio calculation[13b] for primary-to-secondary isomeriza-

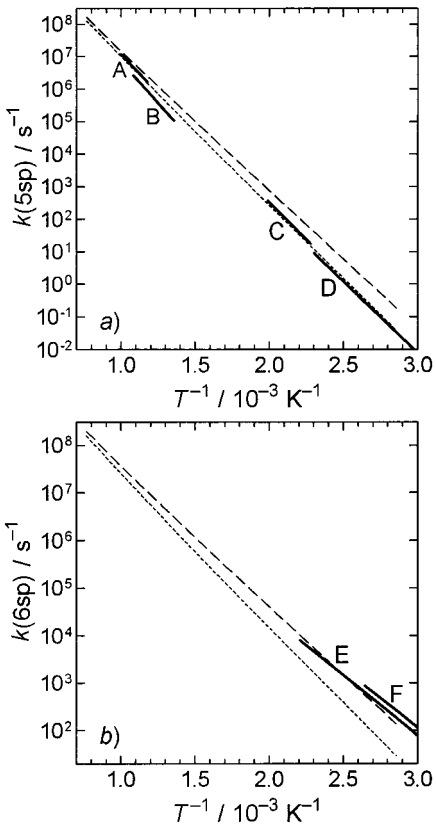

Figure 11. Comparison of the calculated high-pressure limit rate constant with previous low-temperature measurements for (a) five-membered ring isomerization of 1-C_5H_{11} to 2-C_5H_{11} and (b) six-membered ring isomerization of 1-C_6H_{13} to 2-C_6H_{13}. Broken lines (− − −) and dotted lines (- - -) denote the results of TST calculations using present threshold energies, $E_0(5sp) = 20.5$ and $E_0(6sp) = 14.6$ kcal mol^{-1}, with and without Wigner correction, respectively. The bold lines denote the previous measurements by (A) Tsang et al.,[29] (B) Marshall,[10f] (C) Endrenyi and Le Roy[7c] (recalculated by Watkins[10a]), (D) Watkins[9a] (recalculated[10a]), (E) Dóbé et al.,[10e] and (F) Watkins.[10b]

tion, $E_{RS}(5) - E_{RS}(6) = 7.2-8.1$ kcal mol^{-1} (at MP-SAC2 level), and from that[13a] for primary-to-primary isomerization, $E_{RS}(5) - E_{RS}(6) = 7.4$ (at MP-SAC2 level) or 6.3 kcal mol^{-1} (at BAC-MP4 level).

The high-pressure limit rate constants for 5sp and 6sp isomerization reactions calculated by using the threshold energies determined in the present study are compared with previous experimental results[10,27] at lower temperatures in Figure 11. Since the tunneling effect is expected to be large for these hydrogen transfer reactions at lower temperatures, the effect was estimated qualitatively by Wigner correction[28] using imaginary frequencies (2308i and 2265i cm^{-1} for 5sp and 6sp TS's) derived by HF/6-31G(d) calculation. With the tunneling correction, the present $E_0(6sp)$ well reproduces the previous experimental results while the present $E_0(5sp)$ corresponds to the rate constant higher than the previous results. The best fits to the previous measurements give the higher $E_0(5sp)$, 21.5 kcal mol^{-1}. This discrepancy of 1 kcal mol^{-1} may be explained by the effect of the tunneling in the present studies at high temperatures. Since the quantum mechanical effect to the microscopic rate constant is expected to be large at the energies around the threshold energies, the effect of tunneling depends on the population distribution around the threshold energies. As shown in Figure 9, some population in C_5H_{11} is present around the 5sp threshold energy (20.5 kcal mol^{-1}), while almost no population is present around the 6sp threshold energy (14.6 kcal mol^{-1}) in C_6H_{11}, for which the population distribution is similar to C_5H_{11} but slightly shifted toward higher energy by about 5 kcal mol^{-1}. This implies much larger tunneling effect for 5sp isomerization than for 6sp. By ignoring the quantum effect, the present analysis might result in the effectively lower threshold energy for 5sp isomerization. However, no further analysis for the tunneling effect was made since the expected change in the threshold energy (≤1 kcal mol^{-1}) due to the quantum effect is smaller than the error limit (±1.2 kcal mol^{-1}), and the quantitative analysis needs the accurate potential energy curve along the reaction coordinate.

TABLE 1: Estimated High-Pressure Limit Rate Parameters for Straight-Chain Alkyl Radicals at 1000−1300 K

type of reaction	A (per C−H)[a]/ s^{-1}	$E_a - E_0$[a]/ kcal mol^{-1}	E_0[b]/ kcal mol^{-1}
C−H fission (primary radical)	6.9×10^{13}	3.3	∼34.2
C−H fission (secondary radical)	9.3×10^{13}	4.5	∼35.7
C−C fission (primary radical)	1.8×10^{14}	2.1	∼29.2
C−C fission (secondary radical)	3.0×10^{14}	3.3	∼29.5
3sp isomerization	1.6×10^{13}	2.1	∼38.6
4sp isomerization	3.6×10^{12}	2.0	∼38.1
5sp isomerization	3.0×10^{11}	1.3	∼21.5
6sp isomerization	3.4×10^{10}	1.1	∼14.6

[a] A factor and $E_a - E_0$ were derived from the Arrhenius plot of the preexponential part of the TST expression, $(k_BT/h)(Q^{\ddagger}/Q)$, calculated at 1000−1300 K. A factors for C−H fission and isomerization processes were divided by the number of equivalent C−H bonds of concern. Listed values were estimated from (the average of) the rate parameters of typical reaction s, that is, (1) average of •C−C → C═C + H and •CCC → C═CC + H; (2) C−•C−C → C═C−C + H; (3) average of •C−C−C → C═C + •C, •C−C−C−C → C═C + •C−C, •C−C−C−C−C → C═C + •C−C−C, and •C−C−C−C−C−C → C═C + •C−C−C−C; (4) average of C−•C−C−C−C → C−C═C + •C−C, C−•C−C−C−C−C → C−C═C + •C−C−C, and C−C−•C−C−C−C → C−C−C═C + •C−C; (5) •C−C−C → C−•C−C; (6) •C−C−C−C → C−C−•C−C; (7) average of •C−C−C−C−C → C−C−C−•C−C and •C−C−C−C−C−C → C−C−C−•C−C−C; (8) •C−C−C−C−C−C → C−C−C−C−•C−C. [b] Typical threshold energies were estimated, (1) as $\Delta H_0(\sim 32.0) + \sim 2.2$; (2) as $\Delta H_0(\sim 34.9) + \sim 0.8$; (3) as $\Delta H_0(\sim 21.5) + 7.7$; (4) as $\Delta H_0(\sim 21.8) + 7.7$; (5)−(6) from ab initio calculation;[13b] (7)−(8) from present best estimate (see text).

By considering the above discussion, as the best estimate, the threshold energies for the isomerization processes were estimated to be $E_0(5sp) = 21.5$ and $E_0(6sp) = 14.6$ kcal mol^{-1}. By using these, the high-pressure limit rate constants are recommended to be

$$k^{\infty}(5sp) = 4.88 \times 10^8 T^{0.846} \times \exp(-19.53\ [\text{kcal mol}^{-1}]/RT)\ \text{s}^{-1}\ (350-1300\ \text{K})$$

for 5sp isomerization of 1-C_5H_{11} to 2-C_5H_{11}, and

$$k^{\infty}(6sp) = 6.65 \times 10^7 T^{0.823} \times \exp(-12.45\ [\text{kcal mol}^{-1}]/RT)\ \text{s}^{-1}\ (350-1300\ \text{K})$$

for 6sp isomerization of 1-C_6H_{13} to 2-C_6H_{13}. The error limit of these expressions was estimated to be factor of 3. It should be noted that the high-pressure limit assumption is valid only below ∼800 K at 1 atm, where the RRKM calculation suggest that $k(1\ \text{atm})/k^{\infty} \sim 0.7$. No recommendation is made for the rate constants at the high-temperature falloff regime since further experimental and theoretical investigations for the tunneling effect and the nonequilibrium effect are needed for this.

Finally, the general trend of the A factors and activation energies for the relevant decomposition and isomerization processes is discussed. The A factors and the activation energies derived from the TST calculations are summarized in Table 1.

The tunneling correction was not included in the rate parameters in this table. The Wigner correction suggests that the tunneling effect is important for hydrogen-shift isomerization reactions, and the rate constants with tunneling correction can be approximated by lowering threshold energies than those in Table 1 by ~1 kcal mol^{-1}. Although the *A* factors for C−C and C−H fission processed are in the same order (note that the *A* factors for C−H fission processes shown in Table 1 are those "per C−H bond"), the threshold energies for C−H fission processes are higher than those for C−C fission by ~5 kcal mol^{-1} or more. The C−C fission process is generally favored if possible, and the branching fraction for C−H fission process is only ~10% or less at the high-pressure limit. The falloff effect further diminishes the branching fraction for C−H fission, and it will be less than 5% at this temperature range (1000−1300 K) up to 10 atm as shown by the RRKM calculation for *n*-C_3H_7. However, the nonequilibrium effect may increase the branching fraction up to the high-pressure limit, ~10%, as suggested by the present and previous[26] estimations. The threshold energy for intramolecular hydrogen-transfer isomerization reactions decreases as the number of ring members increases, mainly reflecting the decrease of the ring-strain energy, while the *A* factors decreases mainly due to the increasing number of internal rotors inhibited in the ring transition state. Because of the higher threshold energies and smaller *A* factors for 3sp and 4sp isomerization processes than the C−C or C−H fission processes, these processes are expected to be minor, which is consistent with the present experimental results.

Conclusions

In the present study, the product branching fractions for the thermal decomposition of C_3−C_4 alkyl radicals, 1-C_5H_{11}, and 1-C_6H_{13} have been investigated by a shock-tube apparatus with quantitative measurements of hydrogen atoms by ARAS at 900−1400 K and ~1 atm (Ar). Under these conditions, the falloff effect was shown to be important especially in the branching fractions for higher threshold energy channels such as C−H fission processes in competition with C−C fission processes. From the present and previous studies for the isomerization processes, and by considering the possible tunneling effect, the threshold energies for five- and six-membered ring primary-to-secondary (5sp and 6sp) isomerization processes were evaluated to be 21.5 and 14.6 kcal mol^{-1}, respectively. The nonequilibrium effect and the tunneling effect should be investigated by further experimental and theoretical studies.

Appendix

The nascent population distributions of *n*-C_3H_7 radicals produced by reactions R1−R3 (in the subsection C in the Discussion section) were estimated as follows. The partitioning of the excess energy, ϵ^*, into the *n*-C_3H_7 fragment was estimated to be completely statistical, that is, the prior distribution[28] was assumed. The statistical vibrational energy distribution, $g_0(E;\epsilon^*)$, in *n*-C_3H_7 at excess energy ϵ^* can be expressed as,

$$g_0(E;\epsilon^*) = \frac{\rho(E)(\epsilon^* - E)^n}{\int_0^{\epsilon^*} \rho(E)(\epsilon^* - E)^n \, dE}$$

$$n = \frac{n_R + 1}{2} + n_V \qquad \text{(A1)}$$

where $\rho(E)$ is the vibrational density of states of *n*-C_3H_7 at energy E, n_R, and n_V denote the rotational and vibrational degree of freedom to be summed, respectively, that is, the total rotational degree of freedom of two fragments and vibrational degree of freedom of the fragment other than *n*-C_3H_7. Since eq A1 is derived from the replacement of summation over vibrational states by integration, the excess energy, ϵ^*, should be measured from the classical ground state of the fragment other than *n*-C_3H_7 [C_2H_4 for (R2) and H_2O for (R3)]. By using the estimated distribution of ϵ^*, $f^*(\epsilon^*)$, which will be described below, the initial population distribution of *n*-C_3H_7, $g_0(E)$, was calculated as superimposition of $g_0(E;\epsilon^*)$ at different ϵ^*

$$g_0(E) = \int_E^\infty f^*(\epsilon^*) g_0(E;\epsilon^*) \, d\epsilon^* \qquad \text{(A2)}$$

The distribution $f^*(\epsilon^*)$ was estimated as follows. The vibrational energy distribution on the TS of (R1)−(R3), $f_V^{\ddagger}(\epsilon_V^{\ddagger})$, is proportional to the reactive flux above the TS as

$$f_V^{\ddagger}(\epsilon_V^{\ddagger}) \propto g_R(E_0 + \epsilon_V^{\ddagger}) k(\epsilon_V^{\ddagger}) \qquad \text{(A3a)}$$

for unimolecular reactions (R1 and R2), or as,

$$f_V^{\ddagger}(\epsilon_V^{\ddagger}) \propto \rho_V^{\ddagger}(\epsilon_V^{\ddagger}) \exp\left(-\frac{\epsilon_V^{\ddagger}}{k_B T}\right) \qquad \text{(A3b)}$$

for bimolecular reaction (R3), from basic assumptions in RRKM or TST. Here, g_R is the steady-state distribution of the reactant molecule (that is, the steady-state dissociation is assumed for (R1) and (R2)), k is the microscopic rate constant, E_0 is the threshold energy for the dissociation, $\rho_V^{\ddagger}$ is the vibrational density of the state of the TS, k_B is the Boltzmann constant, and T is temperature. By adding the thermal rotational energy, the total energy distribution above the TS, $f^{\ddagger}(\epsilon^{\ddagger})$, is expressed by

$$f^{\ddagger}(\epsilon^{\ddagger}) = \int_0^{\epsilon^{\ddagger}} f_V^{\ddagger}(\epsilon^{\ddagger} - \epsilon_R^{\ddagger}) f_R^{\ddagger}(\epsilon_R^{\ddagger}) \, d\epsilon_R^{\ddagger}$$

$$f_R^{\ddagger}(\epsilon_R^{\ddagger}) = \frac{\rho_R^{\ddagger}(\epsilon_R^{\ddagger}) \exp\left(-\frac{\epsilon_R^{\ddagger}}{k_B T}\right)}{Q_R^{\ddagger}} \qquad \text{(A4)}$$

where $f_R^{\ddagger}$ is the thermal rotational energy distribution, $\epsilon_R^{\ddagger}$ is the rotational energy, $\rho_R^{\ddagger}$ is the rotational density of states, and $Q_R^{\ddagger}$ is the rotational partition function of the transition state. The excess energy distribution, $f^*(\epsilon^*)$, needed to evaluate eq A2 can be derived by adding the energy difference between TS and product, that is, the threshold energy for the reverse reaction, $E_{0,\,rev}$, and the zero-point energy of the fragment other than *n*-C_3H_7, E_{ZP}

$$f^*(\epsilon^*) = 0 \qquad [\epsilon^* < E_{0,\,rev} + E_{ZP}]$$

$$f^*(\epsilon^*) = f^{\ddagger}(\epsilon^* - E_{0,\,rev} - E_{ZP}) \quad [\epsilon^* \geq E_{0,\,rev} + E_{ZP}] \qquad \text{(A5)}$$

The necessary geometry and frequencies of the molecules and TS's were estimated by ab initio calculations similarly to the TST calculation of *n*-C_3H_7 decomposition described in the text.

References and Notes

(1) (a) Slagle, I. R.; Batt, L.; Gmurczyk, G. W.; Gutman, D.; Tsang, W. *J. Phys. Chem.* **1991**, *95*, 7732. (b) Bencsura, Á; Knyazev, V. D.; Xing, S.-B.; Slagle, I. R.; Gutman, D. *Symp. (Int.) Combust., Proc.* **1992**, 24, 629. (c) Feng, Y.; Niiranen, J. T.; Bencsura, Á; Knyazev, V. D.; Gutman, D.; Tsang, W. *J. Phys. Chem.* **1993**, *97*, 871. (d) Seakins, P. W.; Robertson, S. H.; Pilling, M. J.; Slagle, I. R.; Gmurczyk, G. W.; Bencsura, Á.; Gutman,

D.; Tsang, W. *J. Phys. Chem.* **1993**, *97*, 4450. (e) Knyazev, V. D.; Dubinsky, I. A.; Slagle, I. R.; Gutman, D. *J. Phys. Chem.* **1994**, *98*, 5279. (f) Knyazev, V. D.; Dubinsky, I. A.; Slagle, I. R.; Gutman, D. *J. Phys. Chem.* **1994**, *98*, 11099. (g) Knyazev, V. D.; Slagle, I. R. *J. Phys. Chem.* **1996**, *100*, 5318.

(2) Allara, D. L.; Shaw, R. *J. Phys. Chem. Ref. Data* **1980**, *9*, 523.

(3) Dean, A. M. *J. Phys. Chem.* **1985**, *89*, 4600.

(4) Tsang, W. *J. Phys. Chem. Ref. Data* **1988**, *17*, 887.

(5) Tsang, W. *J. Phys. Chem. Ref. Data* **1990**, *19*, 1.

(6) (a) Benson, S. W.; Kistiakowsky, G. B. *J. Am. Chem. Soc.* **1942**, *64*, 80. (b) Kossiakoff, A.; Rice, F. O. *J. Am. Chem. Soc.* **1943**, *65*, 590. (c) Quinn, C. P. *Trans. Faraday Soc.* **1963**, *59*, 2543.

(7) (a) Gordon, A. S.; McNesby, J. R. *J. Chem. Phys.* **1959**, *31*, 853. (b) Gordon, A. S.; McNesby, J. R. *J. Chem. Phys.* **1960**, *33*, 1882. (c) Endrenyi, L.; Le Roy, D. J. *J. Phys. Chem.* **1966**, *70*, 4081.

(8) Benson, S. W. *Thermochemical Kinetics*, 2nd ed.; John Wiley and Sons: New York, 1976.

(9) (a) Watkins, K. W. J. *Am. Chem. Soc.* **1971**, *93*, 6355. (b) Watkins, K. W.; Ostreko, L. A. *J. Phys. Chem.* **1969**, *73*, 2080.

(10) (a) Watkins, K. W. *Can. J. Chem.* **1972**, *50*, 3738. (b) Watkins, K. W. *J. Phys. Chem.* **1973**, *77*, 2938. (c) Le Roy, R. J. *J. Phys. Chem.* **1980**, *84*, 3508. (d) Larson, C. W.; Chua, P. T.; Rabinovitch, B. S. *J. Phys. Chem.* **1972**, *76*, 2507. (e) Dóbé, S.; Bérces, T.; Réti, F.; Márta, F. *Int. J. Chem. Kinet.* **1987**, *19*, 895. (f) Marshall, R. M. *Int. J. Chem. Kinet.* **1990**, *22*, 935.

(11) (a) Heller, C. A.; Gordon, A. S. *J. Phys. Chem.* **1958**, *62*, 709. (b) Kerr, J. A.; Trotman-Dickenson, A. F. *Trans. Faraday Soc.* **1959**, *55*, 921. (c) Kerr, J. A.; Trotman-Dickenson, A. F. *J. Chem. Soc.* **1960**, *1960*, 1602. (d) Jackson, W. M.; McNesby, J. R. *J. Chem. Phys.* **1962**, *36*, 2272. (e) Lin, M. C.; Back, M. H. *Can. J. Chem.* **1966**, *44*, 2369. (f) Tardy, D. C. *Int. J. Chem. Kinet.* **1974**, *6*, 291. (g) Gordon, A. S.; Tardy, D. C.; Ireton, R. *J. Phys. Chem.* **1976**, *80*, 1400. (h) Gierczak, T.; Gawlowski, J.; Niedzielski, J. *React. Kinet. Catal. Lett.* **1988**, *36*, 435.

(12) (a) Harding, L. B. *J. Am. Chem. Soc.* **1981**, *103*, 7469. (b) Dorigo, A. E.; McCarrick, M. A.; Loncharich, R. J.; Houk, K. N. *J. Am. Chem. Soc.* **1990**, *112*, 7508.

(13) (a) Viskolcz, B.; Lendvay, G.; Körtvélyesi, T.; Seres. L. *J. Am. Chem. Soc.* **1996**, *118*, 3006. (b) Viskolcz, B.; Lendvay, G.; Seres, L. *J. Phys. Chem. A* **1997**, *101*, 7119.

(14) Ross, P. L.; Johnston, M. V. *J. Phys. Chem.* **1995**, *99*, 16507.

(15) Koshi, M.; Yoshimura, M.; Fukuda, K.; Matsui, H.; Saito, K.; Watanabe, M.; Imamura, A. *J. Chem. Phys.* **1990**, *93*, 8703.

(16) Kumaran, S. S.; Su, M.-C., Lim, K. P.; Michael, J. V. *Symp. (Int.) Combust., Proc.* **1996**, *26*, 605.

(17) Miyoshi, A.; Yamauchi, N.; Kosaka, K.; Koshi, M.; Matsui, H. *J. Phys. Chem. A* **1999**, *103*, 46.

(18) (a) Tsang, W. *Int. J. Chem. Kinet.* **1978**, *10*, 599. (b) Brow, T. C.; King, K. D.; Nguyan, T. T. *J. Phys. Chem.* **1986**, *90*, 419.

(19) Frisch, M. J.; Trucks, G. W.; Schlegel, H. B.; Gill, P. M. W.; Johnson, B. G.; Robb, M. A.; Cheeseman, J. R.; Keith, T.; Petersson, G. A.; Montgomery, J. A.; Raghavachari, K.; Al-Laham, M. A.; Zakrzewski, V. G.; Ortiz, J. V.; Foresman, J. B.; Cioslowski, J.; Stefanov, B. B.; Nanayakkara, A.; Challacombe, M.; Peng, C. Y.; Ayala, P. Y.; Chen, W.; Wong, M. W.; Andres, J. L.; Replogle, E. S.; Gomperts, R.; Martin, R. L.; Fox, D. J.; Binkley, J. S.; Defrees, D. J.; Baker, J.; Stewart, J. P.; Head-Gordon, M.; Gonzalez, C.; Pople, J. A. *Gaussian 94*, Revision E.1; Gaussian, Inc.: Pittsburgh, PA, 1995.

(20) Foresman, J. B.; Frisch, Æ. *Exploring Chemistry with Electronic Structure Methods*, 2nd ed.; Gaussian, Inc.: Pittsburgh, 1996.

(21) (a) Chase, Jr., M. W.; Davies, C. A.; Downey, Jr., J. R.; Frurip, D. J.; McDonald, R. A.; Syverud, A. N. *JANAF Thermochemical Tables*, 3rd ed.; *J. Phys. Chem. Ref. Data* **1985**, *14*, Supplement No. 1. (b) Atkinson, R.; Baulch, D. L.; Cox, R. A.; Hampson, Jr., R. F.; Kerr, J. A.; Troe, J. *J. Phys. Chem. Ref. Data* **1992**, *21*, 1125.

(22) Gilbert, R. G.; Smith, S. C.; Jordan, M. J. T. *UNIMOL program suite (calculation of falloff curves for unimolecular and recombination reactions)*; 1993, available from the authors: School of Chemistry, Sydney University, NSW 2006, Australia, or by email to: gilbert_r@summer.chem.su.oz.au.

(23) Gilbert, R. G.; Smith, S. C. *Theory of Unimolecular and Recombination Reactions*; Blackwell Scientific Publications: Oxford, UK, 1990.

(24) Tsang, W.; Kiefer, J. R. In *The Chemical Dynamics and Kinetics of Small Radicals, Part I*; Liu, K., Wagner, A., Eds.; World Scientific: Singapore, 1995; p 58.

(25) Bernshtein, V.; Oref, I. *J. Phys. Chem.* **1993**, *97*, 6830.

(26) (a) Tsang, W.; Bedanov, V.; Zachariah, M. R. *J. Phys. Chem.* **1996**, *100*, 4011. (b) Tsang, W.; Bedanov, V.; Zachariah, M. R. *Ber. Bunsen-Ges. Phys. Chem.* **1997**, *101*, 491.

(27) De Avillez Pereira, R.; Baulch, D. L.; Pilling, M. J.; Robertson, S. H.; Zeng, G. *J. Phys. Chem. A* **1997**, *101*, 9681.

(28) Steinfeld, J. I.; Francisco, J. S.; Hase, W. L. *Chemical Kinetics and Dynamics*, Prentice-Hall: Englewood Cliffs, NJ, 1989.

(29) Tsang, W.; Walker, J. A.; Manion, J. A. *Symp. (Int.) Combust., Proc.*, in press.

(30) Wigner, E. *Z. Phys. Chem. (Leipzig)* **1932**, *B19*, 203.